Subunit Conformational Changes Accompanying Bacteriophage P22 Capsid Maturation†

Peter E. Prevelige, Jr.,§ and Dennis Thomas‡

Department of Biology, Massachusetts Institute of Technology, Cambridge, Massachusetts 02139

Kelly L. Aubrey, Stacy A. Towse, and George J. Thomas, Jr.*

School of Biological Sciences, University of Missouri—Kansas City, Kansas City, Missouri 64110-2499

Received May 13, 1992; Revised Manuscript Received October 19, 1992

ABSTRACT: In double-stranded DNA bacteriophages, packaging of dsDNA requires the transformation of a precursor procapsid into a mature viral capsid. Lattice expansion and release of scaffolding subunits accompany DNA packaging. Three-dimensional structures of procapsid and mature phage lattices demonstrate that the capsid transformation involves substantial changes in subunit environment. Since this transformation occurs without subunit dissociation, it represents a transition between at least two stable subunit conformations. Using Raman spectroscopy, we have identified changes in coat protein secondary structure and side-chain environments which accompany the capsid transformation. The subunits of procapsid shells contain only 2.0 ± 0.4% more α-helix and less β-sheet than those of mature capsids; however, numerous side chains are substantially altered by the transformation, including tyrosines, tryptophans, phenylalanines, and aliphatics, which are widely distributed through the subunit sequence. We propose, therefore, that procapsid expansion is accomplished through the relative motion of coat subunit domains with little change in secondary structure. Such hinge-bending conformational transitions may couple ATP-dependent dsDNA condensation with shell expansion.

Assembly of a double-stranded DNA virus requires formation of a metastable and topologically closed precursor particle (procapsid) into which the viral chromosome is ultimately packaged. The procapsid comprises an outer shell of coat protein and an inner core of scaffolding protein. Morphological similarities have been identified for precursor and mature protein shells of adenovirus, herpesvirus, and dsDNA[1] bacteriophages, all of which package a single, linear, dsDNA genome. [For reviews, see Casjens and Hendrix (1988) and Casjens (1989).] A simplified scheme of dsDNA virus morphogenesis is depicted for the case of the *Salmonella* bacteriophage P22 in Figure 1.

For P22 and many other dsDNA bacteriophages, it has been shown that the nucleic acid enters the procapsid through a channel consisting of a dodecameric complex of a specialized minor protein (portal protein), which is located at a unique icosahedral vertex (Bazinet & King, 1985). DNA packaging causes substantial changes to the procapsid coat and scaffolding subunits. The scaffolding protein is eliminated from the shell of coat protein and recycled for further use, while the shell of coat protein undergoes simultaneous increases in both its diameter and its thermostability. In some viruses the release of scaffolding protein and capsid expansion involve covalent modification of the coat protein, although no covalent modification occurs for bacteriophage P22. Conservation of the P22 coat protein primary structure during capsid maturation, together with the availability of three-dimensional reconstructions for both procapsid and mature capsid states (Prasad et al., 1993), makes P22 an ideal system in which to examine possible conformational changes of coat subunits during the assembly process.

Raman vibrational spectroscopy is a convenient probe of molecular conformation and interactions in macromolecular assemblies and is well-suited to comparing structural characteristics of viruses and viral precursors for many different experimental conditions (Thomas, 1987; Li et al., 1990; Prevelige et al., 1990; Bamford et al., 1990; T. Li et al., 1992). Typically, the Raman spectrum of a viral protein assembly consists of about 50 discrete bands which are assignable to vibrational transitions originating from specific nuclear displacements in the subunits (Thomas et al., 1982). In general, the bands are sensitive in frequency (Raman shift in cm^{-1} units) and intensity (Raman cross section in arbitrary units) to the detailed structure and environment of the vibrating molecular subgroups to which they are assigned (Thomas et al., 1983). Key bands of present interest are (i) the amide I and amide III bands, which have their origins in vibrations of the peptide main chain (largely C=O and C–N stretching motions, respectively) and which are diagnostic of secondary structure (Chen & Lord, 1974), and (ii) the bands of tyrosyl, tryptophanyl, and cysteinyl residues, which are diagnostic of side-chain conformation, hydrogen bonding, and hydrophobic interactions (Siamwiza et al., 1975; Miura et al., 1988, 1989; Li & Thomas, 1991; H. Li et al., 1992).

In the present work, we apply Raman spectroscopy to procapsid and capsid assembly states of the major coat subunit (gp5) of bacteriophage P22 (Prevelige et al., 1990). The *procapsid assembly state* is essentially the outer coat protein

† This is Part XXXVII in the series Studies of Virus Structure by Raman Spectroscopy, supported by NIH Grant AI11855 (G.J.T.). Support was also provided by NIH Grants GM47980 (P.E.P.) and GM17980 (Jonathan King).

* Author to whom correspondence should be addressed.

§ Current address: Boston Biomedical Research Institute, 20 Staniford St., Boston, MA 02114.

‡ Current address: Program in Biophysics, Brandeis University, Waltham, MA.

[1] Abbreviations: dsDNA, double-stranded DNA; ATP, adenosine triphosphate; NS, native shell; PS, procapsid shell; EDTA, ethylenediaminetetraacetic acid; SDS–PAGE, sodium dodecyl sulfate–polyacrylamide gel electrophoresis; gp, gene product; TBSV, tomato bushy stunt virus; GuHCl, guanidine hydrochloride.

0006-2960/93/0432-537$04.00/0

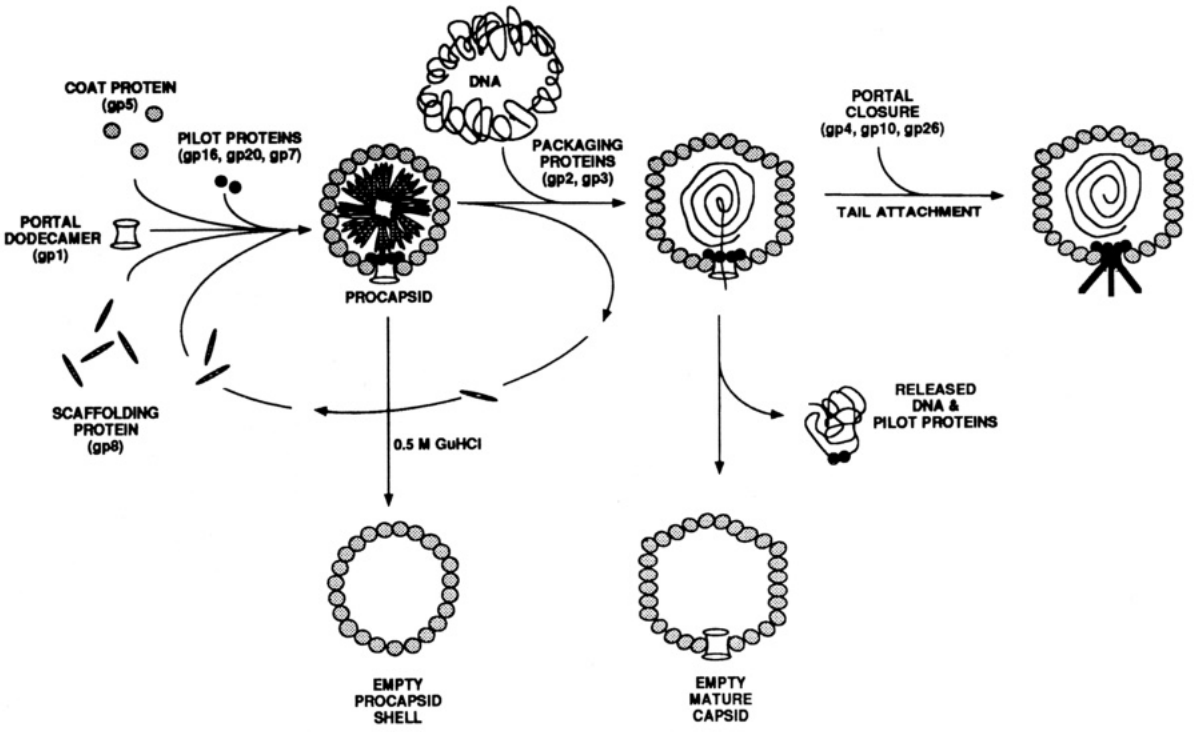

FIGURE 1: Morphogenetic pathway of P22. The gene 5 encoded coat protein copolymerizes in the presence of gene 8 encoded scaffolding subunits, forming a double-shelled procapsid (King et al., 1973; Prevelige et al., 1988). During assembly one vertex is differentiated by incorporation of a dodecamer of the gene 1 encoded portal protein, which forms the channel for DNA translocation (Bazinet et al., 1988). Genomic DNA is packaged into the procapsid by a complex of gene 2 and gene 3 packaging proteins, which dock at the portal vertex (Poteete et al., 1979; Earnshaw & Casjens, 1980). DNA packaging triggers disruption of coat–scaffolding bonds, release of scaffolding protein, and expansion of the capsid lattice (Earnshaw et al., 1976). The released scaffolding protein recycles to participate in further rounds of assembly (King & Casjens, 1974). The capsid, containing newly packaged DNA, is stabilized by three connector proteins (products of genes 4, 10, and 26) added to the portal vertex (Strauss & King, 1984). Binding of tailspikes to the connector complex renders the virions infectious (Israel et al., 1967; Botstein et al., 1973). Vertical arrows indicate the relationships between particles produced in vivo and those used in this study.

shell of the procapsid. It is derived from the procapsid by gentle extraction of the scaffolding protein. This particle is referred to as the empty procapsid shell (or PS). The diameter of the empty procapsid shell is identical to that of the procapsid assembled in vivo (Prasad et al., 1993), which demonstrates that the shell expansion ultimately required for capsid maturation (Figure 1) has not yet taken place. The *capsid assembly state* is the capsid of the native bacteriophage, which we refer to as the native shell (NS). It is derived from a mutant which is unable to completely close the portal vertex following DNA packaging. This allows previously packaged DNA to escape into solution. Since the DNA packaging reaction is coupled with shell expansion (Figure 1), the NS particle exhibits the expanded shell characteristic of the mature capsid. However, because DNA is absent, the Raman spectrum of the NS particle is uncomplicated by bands of the DNA, thus facilitating structural interpretation and quantitative comparison with the nonexpanded PS particle.

This paper describes the Raman signatures of the PS and NS states of the P22 coat protein. The results demonstrate that procapsid and capsid assembly states do not consist of identical gp5 structures. The nature of the observed differences is 2-fold: Accompanying P22 capsid maturation we find, first, that *minor* changes occur in gp5 secondary structure, and second, that *major* changes occur in gp5 side-chain environments, including many altered side-chain interactions. These results are of interest with respect to the general problem of icosahedral capsid maturation in dsDNA viruses. Additionally, the present findings are of interest for comparison with capsid maturation in bacteriophage T4, which, unlike P22, involves a substantial change in subunit secondary structure (Steven et al., 1990).

MATERIALS AND METHODS

(*1*) *Preparation of Empty Procapsid Shells.* Protocols for the preparation of empty procapsid shells (PS) have been described (Prevelige et al., 1988). Briefly, P22 phage carrying an amber mutation in gene 2 (essential for DNA packaging) were used to infect host cells. After 3 h, the cells were collected by centrifugation, lysed by repeated freeze/thawing, and treated with DNase and RNase. Cell debris was removed by low-speed centrifugation, and the procapsids were collected by high-speed centrifugation. The procapsids were extracted three times with 0.5 M GuHCl and finally chromatographed in 0.5 M GuHCl on a Bio-Gel-A 0.5-m column. The procapsids were further concentrated by centrifugation, and exhaustively dialyzed against buffer solution containing 25 mM NaCl, 1 mM EDTA, and 10 mM Tris at pH 7.6.

(*2*) *Preparation of Native Shells.* For the preparation of native shells, devoid of DNA, we employed the mutant P22 phage *4⁻am*1368 (Strauss & King, 1984), which lacks the gene 4 protein required to retain packaged DNA. The infection was carried out as described above. After 3 h, the cells were harvested by centrifugation, lysed, and separated from cell debris by low speed centrifugation. The *4⁻* empty phage particles, as well as contaminating procapsids and phage, were concentrated by centrifugation. One milliliter of the concentrated particles was loaded on a 16-mL 15–30% sucrose gradient and centrifuged at 24 000 rpm for 4.5 h in an SW27.1 rotor at 4 °C. The native shells (sedimentation value S = 170) and purified procapsids which served as standards (S = 240) were centrifuged in parallel. A single well-defined band, which sedimented more slowly than procapsids, was removed and determined by SDS–PAGE analysis to contain >95%

coat protein. The native shells were concentrated by centrifugation and exhaustively dialyzed against 25 mM NaCl, 1 mM EDTA, and 10 mM Tris at pH 7.6. The residual protein in the SDS PAGE profile was distributed between the portal protein (gp1), pilot proteins (gp16 and gp20), and a trace of scaffolding protein (gp8). The morphology of the recovered shells was confirmed by electron microscopy as that of the mature (expanded) empty capsid.

(*3*) *Raman Spectroscopy.* Samples of PS and NS were concentrated by microfiltration or centrifugation to approximately 80–100 mg/mL in 25 mM NaCl, 1 mM EDTA, and 10 mM Tris (pH 7.5). Aliquots of 5–10 μL were transferred to 1-mm glass capillary tubes (Kimax no. 34507), which were sealed and thermostated at 20 °C for spectroscopic examination. Instrumentation for Raman spectroscopy and data collection protocols have been described (Li et al., 1990; Prevelige et al., 1990). Briefly, all spectra were excited with the argon 514.5-nm line and collected on a scanning spectrophotometer (Spex Ramalog V/VI) under computer control. Raman amide I spectra in the region 1500–1750 cm^{-1} were collected as averages of 30 scans, and survey spectra in the region 600–1750 cm^{-1}, as averages of eight scans. These data were compensated for the very weak Raman scattering of H_2O at ca. 1640 cm^{-1}. Spectra of the sulfhydryl region, 2500–2600 cm^{-1}, were collected as averages of 50 or more scans. All spectra were recorded with scanning increment of 1 cm^{-1}, photon-counting integration time of 1.5 s, and laser power of 200 mW or less at the sample. The experiments were performed in triplicate (PS) or duplicate (NS) on independently prepared samples, and the results were identical within the limits of precision of the measurements, i.e., within ±0.5% in amide I intensities and ±0.5 cm^{-1} in amide I frequencies. For weaker Raman bands, larger limits exist in the reproducibilities of intensities (1–4%) and frequencies (±1.0 cm^{-1}). The spectrometer wavenumber drive was calibrated with liquid indene, and frequency alignment to within ±0.5 cm^{-1} was verified before and after spectra were recorded with the usual secondary standards (CCl_4 459-cm^{-1} and phenylalanine 1002-cm^{-1} line).

RESULTS AND DISCUSSION

Raman spectroscopy is well-suited to detecting small changes of subunit secondary structure in protein assemblies (Thomas, 1987). The method depends upon the sensitivity of key spectral markers—amide I and amide III bands—to changes in protein secondary structure (Chen & Lord, 1974). Specific types of side-chain hydrogen bonding and conformation are also revealed by other Raman bands for which structural correlations have been established through appropriate analyses of model compounds (Siamwiza et al., 1975; Miura et al., 1988, 1989; Li & Thomas, 1991). [For reviews of earlier work, see the monograph edited by Spiro (1987).]

Previously, we applied Raman spectroscopy to demonstrate a small difference between secondary structures of P22 coat protein subunits in two distinct assembly states, viz., empty procapsid shells (similar to the PS defined here) and aberrantly associated subunits (Prevelige et al., 1990). Since the latter do not form topologically closed shells, we noted that the observed secondary structure difference has the potential for discriminating incorrect and correct capsid assembly pathways. In the earlier study, we found also that gentle heat treatment (above 37 °C) was helpful to catalyze polymerization of gp5 into the aberrantly associated subunits, and accordingly, a similar heat-treatment protocol was applied to the empty procapsid shells with which the aberrantly associated subunits

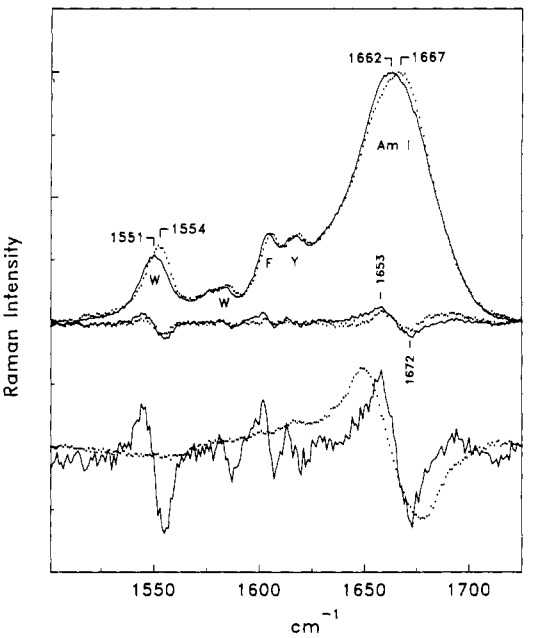

FIGURE 2: (Top) Raman amide I spectra of empty procapsid shells (—) and native shells (···). Each is the average of 30 scans. Labels identify Raman band centers and residues to which they are assigned (AmI = amide I, W = tryptophan, Y = tyrosine, F = phenylalanine). (Middle) Difference spectrum computed with empty procapsid shell as minuend and native shell as subtrahend (—). Included is the difference spectrum (···) obtained after applying abscissa shifts of +0.5 cm^{-1} to the empty procapsid and −0.5 cm^{-1} to the native shell. Similar results were obtained for oppositely signed shifts (data not shown), demonstrating that observed differences are not due to misalignments within ±1.0 cm^{-1} of either minuend or subtrahend. (Bottom) Five-fold amplification of the observed difference spectrum (—) superposed with the model helix-minus-sheet [Pf1 minus β-poly(L-serine)] difference spectrum (···). Other details of data collection are given in the text.

were compared. Our previous paper (Prevelige et al., 1990), therefore, reports a structural comparison specific to heat-treated specimens. Here we have avoided heat treatment of NS and PS, thus maintaining sample handling conditions as close as possible to those used in parallel electron cryomicroscopy experiments (Prasad et al., 1993), which demonstrate by three-dimensional image reconstructions that extraction of the scaffolding protein with 0–5 mM GuHCl does not significantly perturb the coat protein lattice.

In the analysis which follows, we make use of established Raman spectra–structure correlations (Spiro, 1987) to assess secondary structures and side-chain characteristics of coat protein subunits in empty procapsid shells (PS) and native shells (NS), not subjected to either heat or chemical treatments.

(*1*) *Main-Chain Vibrations.* The top traces of Figure 2 show the Raman amide I spectra of empty procapsid shells (PS, solid line) and native shells (NS, dotted line). The spectra are distinguished by a small but reproducible difference in the amide I peak, which is centered at 1662 cm^{-1} in PS and at 1667 cm^{-1} in NS. These and all peak frequencies for intense bands are reproducibly measured to ±0.5 cm^{-1}. The PS and NS spectra also exhibit reproducible differences in their tryptophan (W) band near 1552 cm^{-1}. In PS, the W band is centered at 1551 cm^{-1} and is weaker than the NS counterpart, which is centered at 1554 cm^{-1}. Smaller and close to marginal differences are evident in the region 1580–1620 cm^{-1} where overlapping bands are assigned to tryptophan (W), phenylalanine (F), and tyrosine (Y) residues. The spectral differences between PS and NS are clearly revealed in the digitally

computed difference spectrum of Figure 2 (PS-minus-NS, middle trace, solid line), which is shown on the same ordinate scale as those of PS and NS. In this computation, the positive and negative lobes of the amide I difference are of equal magnitude with extrema at 1653 and 1672 cm^{-1}, respectively.

In order to confirm that the difference in Figure 2 between amide I bands of PS and NS is not an artifact of abscissa misalignment, we have arbitrarily shifted the two spectra closer to one another by 1 cm^{-1} (the sum of uncertainties in spectral wavenumber calibration in the two spectra) and recomputed the difference. The result is shown as a dotted line in the middle trace of Figure 2. It is clear that a full 1-cm^{-1} shift of either spectrum, or equivalently, an 0.5-cm^{-1} shift of both spectra toward a common center, does not eliminate the distinctions in either the amide I band center, ca. 1665 cm^{-1}, or in the tryptophan band center, ca. 1552 cm^{-1}. We have also confirmed that larger shifts and opposite-sign shifts of PS and NS do not alter the basic features of the computed difference spectrum.

The lower trace of Figure 2 displays a 5-fold expansion of the PS-minus-NS difference spectrum (solid line). Also shown on the same scale is a computed difference spectrum between model α-helix and β-sheet secondary structures (dotted line). For this computation, we employed as the α-helix model (minuend) the filamentous phage Pf1, which consists predominantly of an α-helical coat protein. For the β-sheet model (subtrahend), we employed β-poly(L-serine). Further discussion of the Raman spectra of these model systems is given elsewhere (Thomas et al., 1987). The qualitative similarities of the PS-minus-NS and helix-minus-sheet amide I differences are evident in the lower traces of Figure 2 and confirm the nature of the net subunit secondary structure change accompanying transformation of the procapsid shell to the native shell. *The empty procapsid shell is richer in α-helix; the native shell is richer in β-sheet.*

In order to obtain a quantitative estimate of the secondary structure change indicated in Figure 2, we measured the fractional intensity change in the total amide I band area which is contributed by the amide I difference lobes. In computing the total Raman amide I band area, we assumed a symmetrical band shape and compensated for equivalent contributions to the overall band intensity expected from the 95 side-chain carbonyls, 25N + 32D + 18Q + 20E, of the gp5 sequence (Eppler et al., 1991). In computing the areas of the difference lobes, we imposed a horizontal baseline through the natural noise level defined by the high- and low-frequency asymptotes (Figure 2). We obtained from this calculation a minimum subunit secondary structure change of 2.0% α-helix in PS to 2.0% β-sheet in NS. Both of these values have an estimated absolute uncertainty of $\pm$0.4%, which results primarily from the $\pm$0.5-cm^{-1} imprecision in spectral abscissa alignments.

The Raman amide I band shift measured from the data of Figure 2 provides a lower limit to the magnitude of the secondary structure change. This is a consequence of the inherent broadness of the helix and sheet amide I band components, which overlap considerably (25–50%) even in the case of ideal α-helix and β-sheet models (Thomas et al., 1987). Accordingly, the data of Figure 2 and the computation described above may fail to detect an additional 0.5–1.0% of residues involved in the $\alpha \rightarrow \beta$ transition. We note also that the Raman amide I band envelope, in the cases of both PS (1662 cm^{-1}) and NS (1667 cm^{-1}), is centered within the interval 1660–1680 cm^{-1}, which is as expected for a protein containing β-strand as the major secondary structure component (Chen & Lord, 1974; Sargent et al., 1988). A β-rich secondary structure for gp5 is consistent with the protein folds revealed by X-ray crystallography in subunits of most icosahedral viral capsids (Rossmann & Johnson, 1989). Prediction algorithms also suggest that the gp5 sequence (Eppler et al., 1991) favors β-strand secondary structure (data not shown).

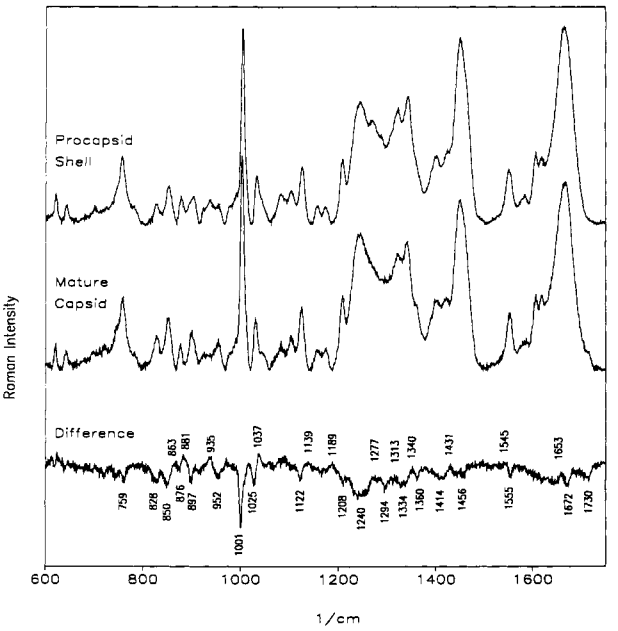

FIGURE 3: Raman spectra in the region 600–1750 cm^{-1} of empty procapsid shells (PS) and native shells (NS). Each spectrum is the average of eight scans. Other details of data collection are given in the text. The bottom trace shows a 2-fold amplification of the computed difference spectrum. Labels identify band centers in cm^{-1} units; detailed assignments are given elsewhere (Prevelige et al., 1990). Several environment-sensitive bands of tryptophan and tyrosine are discussed in the text. Changes in environment are apparent also for bands assigned to phenylalanine (1002 and 1030 cm^{-1}) and aliphatic side chains (ca. 900, 1100, and 1300–1470 cm^{-1}). Not apparent at this spectral amplification is the small but significant shift of the tryptophan hydrogen-bonding marker from 877 cm^{-1} in empty procapsid shells to 875 cm^{-1} in mature capsids, signifying a weaker 1N–H donor in the former.

Figure 3 shows significant differences between Raman spectra of PS and NS in the spectral regions of conformation-sensitive amide III bands (1230–1300 cm^{-1}) and skeletal Cα–Cβ stretching (930–960 cm^{-1}) vibrations. Amide III in PS displays a prominent shoulder at 1272 cm^{-1} and a lesser shoulder near 1300 cm^{-1}. Both of these features are associated with α-helix secondary structure (Chen & Lord, 1974; Thomas et al., 1986) and both are diminished in NS. Conversely, amide III in NS exhibits greater intensity near 1235–1240 cm^{-1}, which is the interval associated with β-sheet secondary structure (Chen & Lord, 1974; Sargent et al., 1988), thus indicating a greater percentage of β-sheet structure in NS than in PS. Finally, we note that in the region of conformation-sensitive Cα–Cβ stretching modes, PS exhibits greater intensity than NS for the band at 935 cm^{-1}, which is diagnostic of side chains incorporated into α-helical domains (Thomas et al., 1986). These results are qualitatively and quantitatively consistent with Figure 2.

(*2*) *Side-Chain Vibrations.* The Raman spectra of PS and NS shown in Figure 3 (600–1750-cm^{-1} interval) and Figure 4 (2500–2650-cm^{-1} interval) contain a large number of bands due to vibrations of specific amino acid side chains of gp5. Assignments for those of Figure 3 have been reported previously (Thomas et al., 1982; Prevelige et al., 1990). In Figure 4, the weak band at 2572 cm^{-1} is due to the sulfhydryl

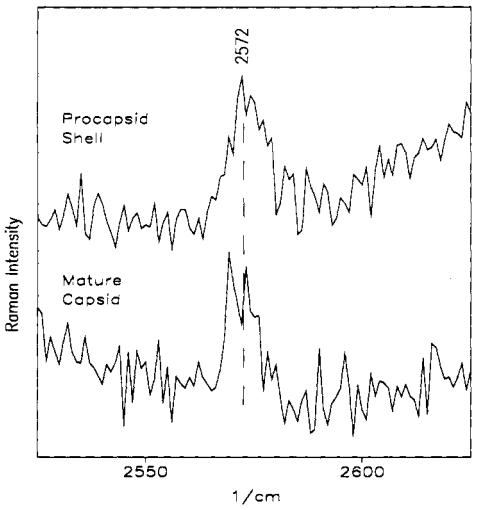

FIGURE 4: Raman SH stretching bands of empty procapsid shells (PS) and native shells (NS). Each spectrum is the average of 50 scans.

stretching vibration of the single cysteine residue (C405) in each gp5 subunit (Eppler et al., 1991). Figure 3 shows that most Raman bands of gp5 are affected in frequency or intensity, or both, by the PS → NS transformation. Here we confine discussion to a few key bands of specific residue types, viz., tyrosine, tryptophan and cysteine, for which the observed frequencies and/or intensities can be reliably correlated with side-chain hydrogen bonding states or residue orientations.

In addition to the band at ca. 1552 cm^{-1} (Figure 2), the six tryptophan residues of gp5 (W48, W61, W145, W241, W354, and W410) give rise to a well-resolved band at 875 cm^{-1} as well as a weak shoulder at 1360 cm^{-1}. The band which is centered at 875 cm^{-1} in NS occurs at slightly higher frequency (877 cm^{-1}) in PS, and the shoulder at 1360 cm^{-1} is clearly more intense in the NS spectrum than in the PS spectrum. Similarly, Figures 2 and 3 show that the 1554-cm^{-1} band of NS is more intense than its counterpart (1551 cm^{-1}) in PS. Harada and co-workers (Miura et al., 1988, 1989) have established correlations of these band positions and intensity shifts with changes in hydrogen bonding and orientation of the indole ring. Thus, we may interpret the shift to higher frequency of the 875-cm^{-1} band of NS as evidence of somewhat weaker hydrogen bonding of the average indole 1N–H donor group in PS than in NS. The diminished intensity of the 1360-cm^{-1} shoulder in PS vs NS reflects on average a more hydrophilic environment for the indole rings of PS. Precisely the same Raman band shifts are observed to accompany LiBr treatment of aqueous lysozyme (Miura et al., 1988), a protein which also contains six tryptophans. Finally, the shift of the 1554-cm^{-1} band in NS to 1551 cm^{-1} in PS reflects a change in orientation of the tryptophan side chain, corresponding to a reduction in magnitude of the side-chain torsion angle $\chi^{2,1}$ (C2–C3–Cβ–Cα torsion) from ca. 105° in NS to ca. 90° in PS (Miura et al., 1989). We emphasize that the Raman bands monitor all six W residues collectively and therefore the above interpretation refers to the configuration of the average W residue.

The eight tyrosines of gp5, viz., Y33, Y100, Y168, Y175, Y180, Y196, Y327, and Y411 (Eppler et al., 1991), generate the Fermi doublet at 827 and 851 cm^{-1}, for which the intensity ratio (I_{851}/I_{827}) is indicative of the state of hydrogen bonding of the tyrosyl OH groups (Siamwiza et al., 1975). Signal-averaged data (not shown) indicate that I_{851}/I_{827} increases from 1.4 in NS to 1.9 in PS, corresponding to a significant change in hydrogen bonding. The value of 1.4 in NS indicates that phenolic groups of native-shell subunits are involved nearly equally as both hydrogen-bond donors and acceptors, while the value of 1.9 in PS identifies phenolic groups of empty-procapsid-shell subunits as being involved predominantly as hydrogen-bond donors. Raman bands of tyrosine occur also at 644, 1208, and 1268 cm^{-1} and these likewise exhibit intensity differences between PS and NS, confirming changes in the tyrosine environments.

The gp5 subunit contains 17 phenylalanine residues, dispersed widely through the sequence (F86, F87, F147, F156, F169, F170, F188, F208, F236, F256, F275, F280, F295, F353, F373, F381, and F392) (Eppler et al., 1991). All contribute to the distinctive Raman bands of the phenylalanine side chain at 621, 1002, 1031, and 1605 cm^{-1} (Prevelige et al., 1990). The 1002-cm^{-1} band is the strongest in the NS spectrum, but in PS its peak height is significantly attenuated (≈30%) and its half-width is marginally increased vis-a-vis NS. Slight broadening is also evident in the phenylalanine Raman markers of PS at 621 and 1031 cm^{-1} compared with those of NS. Although the structural significance of these Raman intensity changes is not known in detail, they indicate that the average molecular environment of F residues is not identical for PS and NS states. By analogy with Raman hypochromic effects observed for other aromatic residues (Small & Peticolas, 1971; Thomas et al., 1971), we may infer that the phenyl ring environments are less uniform in PS than in NS particles. This is consistent with greater solvent exposure, on average, of the phenylalanyl side chains in the procapsid shells.

Other band width and intensity changes in the 700–1500-cm^{-1} interval (Figure 3) confirm maturation-induced changes in side-chain environments and again suggest greater variety in side-chain environments for procapsid shells than for mature capsids (Thomas, 1987; Thomas et al., 1987; Prevelige et al., 1990).

However, not all Raman bands associated with side chains are altered significantly by shell expansion. Figure 4 shows, for example, that the Raman SH stretching band at 2572 cm^{-1} is present in both PS and NS. The SH band is extraordinarily weak, consistent with the occurrence of only a single cysteine (C405) in gp5 (Eppler et al., 1991). Nevertheless, no other interfering Raman bands occur in this spectral interval and the assignment to C405 is unambiguous. The near constancy of the band center at 2572 cm^{-1} indicates a moderately strong S–H···X hydrogen bond donated by the C405 sulfhydryl in subunits of both PS and NS (Li & Thomas, 1991). The relatively low signal-to-noise ratio of Figure 4 does not warrant detailed comment on the SH band shape, although it is apparently not greatly affected by the PS → NS transition. The virtual invariance of the Raman SH frequency (2572 cm^{-1}) to the PS → NS transition suggests that the carboxy-terminal region of the gp5 subunit may not be involved in secondary or tertiary structure changes associated with capsid maturation.

CONCLUSIONS

The results of this study indicate that the procapsid to capsid transformation of the *Salmonella* bacteriophage P22 involves a small change in coat protein secondary structure and pronounced changes in many side-chain interactions and environments. Because the altered side chains are distributed widely through the gp5 sequence and because icosahedral symmetry is conserved, it is unlikely that the associated tertiary structure changes are highly localized either within a given

subunit or among a small number of subunits of the capsid. The pattern of pronounced changes in side-chain environments without large changes in secondary structure is consistent with a transformation involving displacive domain movement in subunits (Rossmann, 1984).

The specific changes in side-chain environments indicated for the PS → NS transformation, including the increased hydrophobicity of tryptophan indoles and the greater imbalance between acceptor and donor roles of tyrosine phenoxyls, are consistent with a decrease in solvent exposure of side chains accompanying maturation. Domain movements which decrease the accessibility of solvent to lattice sites could occur by increasing either intrasubunit or intersubunit contacts following maturation. The three-dimensional structures of the procapsid and capsid forms reveal that a hole located at the center of each hexameric coat protein cluster is closed upon maturation, necessitating new subunit contacts (Prasad et al., 1993). Besides new subunit contacts at the 6-fold axes, additional intersubunit contacts are formed at the 2-fold axes (Prasad et al., 1993). Therefore, the solvent shielding implied by Raman spectroscopy to accompany maturation could be due to formation of the same contacts visualized by electron cryomicroscopy.

Domain movements have been invoked to explain the expansion of plant virus and bacteriophage λ capsids (Robinson & Harrison, 1982; Kawaguchi et al., 1983). For λ, a change in tyrosine solvent exposure upon expansion occurs without change in secondary structure. The X-ray structures of expanded and contracted forms of TBSV confirm that conserved domains are swiveled by hinge movements (Robinson & Harrison, 1982). In contrast, a recent study of bacteriophage T4 polyheads demonstrates that T4 capsid expansion is accompanied by a change in secondary structure more than 10 times larger (≈25%) than that observed here for P22 (Steven et al., 1990). One unique difference between bacteriophage T4 and the other viruses studied is that proteolytic cleavage of the coat protein accompanies T4 capsid expansion.

The procapsid lattice transforms to the mature capsid lattice by displacive domain movement without subunit dissociation. Electron cryomicroscopy and Raman spectroscopy show that subunits are in different overall conformations in the two lattices. Although both subunit conformers are stable under identical solution conditions, a considerable kinetic or energetic barrier must exist between them, evidenced by the pathway dependency and irreversibility of the transformation. Within cells, the transformation is initiated by DNA packaging, which requires continuing ATP hydrolysis (Black, 1989). Some of this chemical energy may be utilized to drive the transformation, liberating a latent bonding potential in the subunits. Similar conformational switching has been described for transformations of screw character in bacterial flagella (Asakura & Ino, 1972). More complex lattice-associated conformational transitions also underlie muscle contraction (Hibberd & Trentham, 1986). The P22 subunit transition, triggered by DNA packaging and driven by ATP hydrolysis, may reflect a general mechanism for in vivo translation of chemical energy into mechanical motion. Further investigations are in progress to elucidate the specific subunit domains involved in the gp5 structure transformations, including those resulting from in vivo maturation and in vitro heat treatment of procapsids.

ACKNOWLEDGMENT

The support of this research by NIH Grants AI11855 (G.J.T.) and GM47980 (P.E.P.) is gratefully acknowledged. We thank Professor Jonathan King, Department of Biology, MIT, for providing helpful comments on the manuscript, facilities for phage protein isolations, and financial support for P.E.P. and D.H.T. through NIH Grant GM17980.

REFERENCES

Asakura, S., & Ino, T. (1972) *J. Mol. Biol. 64*, 251–268.
Bamford, D. H., Bamford, J. K. H., Towse, S. A., & Thomas, G. J., Jr. (1990) *Biochemistry 29*, 5982–5987.
Bazinet, C., & King, J. (1985) *Annu. Rev. Microbiol. 39*, 109–129.
Bazinet, C., Benbasat, J., King, J., Carazo, J., & Carrascosa, J. (1988) *Biochemistry 27*, 1849–1856.
Botstein, D., Waddell, C. H., & King, J. (1973) *J. Mol. Biol. 80*, 669–695.
Black, L. (1989) *Annu. Rev. Microbiol. 43*, 267–292.
Casjens, S. (1989) in *Chromosomes, Eukaryotic, Prokaryotic and Viral*, (Adolph, K. W., Ed.) Vol. III, pp 241–261, CRC Press, Boca Raton, FL.
Casjens, S., & Hendrix, R. (1988) in *The Bacteriophages*, (Calendar, R., Ed.) Vol. 1, pp 15–91, Plenum, New York.
Chen, M. C., & Lord, R. C. (1974) *J. Am. Chem. Soc. 96*, 4750–4752.
Earnshaw, W., & Casjens, S. (1980) *Cell 21*, 319–331.
Earnshaw, W., Casjens, S., & Harrison, S. C. (1976) *J. Mol. Biol. 104*, 387–410.
Eppler, K., Wyckoff, E., Goates, J., Parr, R., & Casjens, S. (1991) *Virology 183*, 519–538.
Fuller, M. T., & King, J. (1981) *Virology 112*, 529–547.
Hibberd, M. G., & Trentham, D. R. (1986) *Annu. Rev. Biophys. Biophys. Chem. 15*, 119–161.
Israel, J. V., Anderson, T. F., & Levine, M. (1967) *Proc. Natl. Acad. Sci. U.S.A. 57*, 284–291.
Kawaguchi, K., Noda, H., & Katsura, I. (1983) *J. Mol. Biol. 164*, 573–587.
King, J., & Casjens, S. (1974) *Nature 251*, 112–119.
King, J., Lenk, E. V., & Botstein, D. (1973) *J. Mol. Biol. 80*, 697–731.
Li, H., & Thomas, G. J., Jr. (1991) *J. Am. Chem. Soc. 113*, 456–462.
Li, H., Wurrey, C. J., & Thomas, G. J., Jr. (1992) *J. Am. Chem. Soc. 114*, 7463–7469.
Li, T., Chen, Z., Johnson, J. E., & Thomas, G. J., Jr. (1990) *Biochemistry 29*, 5018–5026.
Li, T., Chen, Z., Johnson, J. E., & Thomas, G. J., Jr. (1992) *Biochemistry 31*, 6673–6682.
Miura, T., Takeuchi, H., & Harada, I. (1988) *Biochemistry 27*, 88–94.
Miura, T., Takeuchi, H., & Harada, I. (1989) *J. Raman Spectrosc. 20*, 667–671.
Poteete, A. R., Jarvik, V., & Botstein, D. (1979) *Virology 95*, 550–564.
Prasad, B. V. V., Prevelige, P. E., Marietta, E., Chen, R. O., Thomas, D., King, J., & Chiu, W. (1993) *J. Mol. Biol.* (in press).
Prevelige, P., Thomas, D., & King, J. (1988) *J. Mol. Biol. 202*, 743–757.
Prevelige, P. E., Jr., Thomas, D., King, J., Towse, S. A., & Thomas, G. J., Jr. (1990) *Biochemistry 29*, 5626–5633.
Robinson, I. K., & Harrison, S. C. (1982) *Nature 297*, 563–568.
Rossmann, M. G. (1984) *Virology 134*, 1–13.
Rossmann, M. G., & Johnson, J. E. (1989) *Annu. Rev. Biochem. 58*, 533–573.
Sargent, D., Benevides, J. M., Yu, M.-H., King, J., & Thomas, G. J., Jr. (1988) *J. Mol. Biol. 199*, 491–502.
Siamwiza, M. N., Lord, R. C., Chen, M. C., Takamatsu, T., Harada, I., Matsuura, H., & Shimanouchi, T. (1975) *Biochemistry 14*, 4870–4876.
Small, E. W., & Peticolas, W. L. (1971) *Biopolymers 10*, 69–88.

Spiro, T. G., Ed. (1987) *Biological Applications of Raman Spectroscopy, Vol. 1, Raman Spectra and the Conformations of Biological Macromolecules*, Wiley-Interscience, New York.
Steven, A. C., Greenstone, H., Bauer, A. C., & Williams, R. W. (1990) *Biochemistry 29*, 5556–5561.
Strauss, H., & King, J. (1984) *J. Mol. Biol. 172*, 523–543.
Thomas, G. J., Jr. (1987) in *Biological Applications of Raman Spectroscopy, Vol. 1, Raman Spectra and the Conformations of Biological Macromolecules*, (Spiro, T. G., Ed.) pp 135–201, Wiley-Interscience, New York.
Thomas, G. J., Jr., Medeiros, G. C., & Hartman, K. A. (1971) *Biochem. Biophys. Res. Commun. 44*, 587–592.
Thomas, G. J., Jr., Li, Y., Fuller, M. T., & King, J. (1982) *Biochemistry 21*, 3866–3878.
Thomas, G. J., Jr., Prescott, B., & Day, L. A. (1983) *J. Mol. Biol. 165*, 321–356.
Thomas, G. J., Jr., Prescott, B., Benevides, J. M., & Weiss, M. A. (1986) *Biochemistry 25*, 6768–6778.
Thomas, G. J., Jr., Prescott, B., & Urry, D. W. (1987) *Biopolymers 26*, 921–934.